Parameter estimation biases due to contributions from the Rees–Sciama effect to the integrated Sachs–Wolfe spectrum

Björn Malte Schäfer,[1,2]★ Angelos Fotios Kalovidouris[2] and Lavinia Heisenberg[3,4]

[1]*Institut d'Astrophysique Spatiale, Université Paris XI, bâtiment 120-121, Centre universitaire d'Orsay, 91440 Orsay Cedex, France*
[2]*Astronomisches Recheninstitut, Zentrum für Astronomie, Universität Heidelberg, Mönchhofstraße 12, 69120 Heidelberg, Germany*
[3]*Institut für theoretische Astrophysik, Zentrum für Astronomie, Universität Heidelberg, Albert-Ueberle-Straße 2, 69120 Heidelberg, Germany*
[4]*Département de physique théorique, Université de Genève, 24, quai Ernest Ansermet, 1211 Genève, Switzerland*

ABSTRACT

The subject of this paper is an investigation of the non-linear contributions to the spectrum of the integrated Sachs–Wolfe (iSW) effect. We derive the corrections to the iSW autospectrum and the iSW-tracer cross-spectrum consistently to third order in perturbation theory and analyse the cumulative signal-to-noise ratio for a cross-correlation between the *Planck* and *Euclid* data sets as a function of multipole order. We quantify the parameter sensitivity and the statistical error bounds on the cosmological parameters Ω_m, σ_8, h, n_s and w from the linear iSW effect and the systematical parameter estimation bias due to the non-linear corrections in a Fisher formalism, analysing the error budget in its dependence on multipole order. Our results include the following: (i) the spectrum of the non-linear iSW effect can be measured with 0.8σ statistical significance, (ii) non-linear corrections dominate the spectrum starting from $\ell \simeq 10^2$, (iii) an anticorrelation of the CMB temperature with tracer density on high multipoles in the non-linear regime, (iv) a much weaker dependence of the non-linear effect on the dark energy model compared to the linear iSW effect and (v) parameter estimation biases amount to less than 0.1σ and weaker than other systematics.

Key words: cosmic background radiation – cosmological parameters – large-scale structure of Universe.

1 INTRODUCTION

The integrated Sachs–Wolfe (iSW) effect (Sachs & Wolfe 1967; Hu & Sugiyama 1994; Cooray 2002), which refers to the frequency change of cosmic microwave background (CMB) photons if they cross time-evolving gravitational potentials, is a direct probe of dark energy because it vanishes in cosmologies with $\Omega_m = 1$ (Crittenden & Turok 1996). By now, it has been detected with high significance with a number of different tracer objects (Fosalba, Gaztañaga & Castander 2003; Boughn & Crittenden 2004; Nolta et al. 2004; Padmanabhan et al. 2005; Cabré et al. 2006; Gaztañaga, Manera & Multamäki 2006; Giannantonio et al. 2006; Pietrobon, Balbi & Marinucci 2006; Vielva, Martínez-González & Tucci 2006; McEwen et al. 2007; Rassat et al. 2007; Giannantonio et al. 2008), and derived parameter constraints provide support for a Λ cold dark matter (ΛCDM) cosmology.

Contrarily, the non-linear iSW effect or Rees–Sciama (RS) effect (Rees & Sciama 1968; Seljak 1996; Schäfer & Bartelmann 2006) is difficult to detect and shows only a weak signal amounting to $<2\sigma$ in the spectrum (Cooray 2002) or up to 0.8σ in the bispectrum (Schäfer 2008). The cross-correlation with weak lensing has been shown to

be feasible, but weak with current surveys (Nishizawa et al. 2008). In comparison to the linear iSW effect, the RS effect shows a flatter spectral dependence and dominates the signal at higher multipoles exceeding $\ell \gtrsim 100$. Analytically, perturbative derivations agree well with the results from *N*-body simulations (Tuluie, Laguna & Anninos 1996; Cai et al. 2008; Smith, Hernandez-Monteagudo & Seljak 2009; Cai et al. 2010). The non-Gaussianities introduced into the CMB by the non-linear RS effect are very weak (Mollerach et al. 1995; Munshi, Souradeep & Starobinsky 1995; Spergel & Goldberg 1999; Goldberg & Spergel 1999, although the first two papers work in the context of a standard cold dark matter (SCDM) cosmology, their results are still applicable to ΛCDM). The RS effect from the local Universe has been found to amount to ∼2 μK in the most massive structures (Maturi et al. 2007) forming in a constraint realization.

The topic of this paper is the contamination of the iSW spectrum by the non-linear RS spectrum at intermediate multipoles. In a measurement of the linear iSW effect, non-linear contributions will alter the shape of the observed spectrum and can affect the estimation of cosmological parameters by introducing estimation biases. We investigate dependence of parameter accuracy as well as the parameter estimation bias as a function of maximum multipole order considered. Specifically, we use a Fisher-matrix approach to quantify the statistical and systematical errors, analyse the error

★E-mail: spirou@ita.uni-heidelberg.de

budget as a function of multipole order and derive the optimal maximum multipole moment which minimizes the combined error for individual parameters. The non-linear iSW effect is the most important contaminant at intermediate multipoles, with the kinetic Sunyaev–Zel'dovich effect starting to dominate at higher multipoles above 1000 (da Silva et al. 2001; Springel, White & Hernquist 2001; Cooray & Sheth 2002).

After summarizing key formulae describing structure formation in dark energy cosmologies in Section 2, we introduce line-of-sight expressions of the two relevant observables in Section 3. We carry out a perturbative expansion of the source fields to third order in Section 4 and derive the spectrum $C_{\tau\gamma}(\ell)$ between iSW temperature perturbation τ and the galaxy density γ to third order in Section 5. We quantify the degeneracies between the cosmological parameters using a Fisher-matrix analysis in Section 6 and extend this formalism to describe the parameter estimation bias in Section 7. A summary of our results is compiled in Section 8.

As cosmologies, we consider spatially flat homogeneous dark energy models with constant dark energy equation of state and with Gaussian adiabatic initial conditions in the CDM field. Specific parameter choices for the wCDM fiducial model in the Fisher-matrix analysis are $H_0 = 100\,h\,\mathrm{km\,s^{-1}\,Mpc^{-1}}$ with $h = 0.72$, $\Omega_m = 0.25$, $\Omega_b = 0.04$, $\sigma_8 = 0.8$, $w = -0.9$ and $n_s = 1$, with a constant unit bias for the tracer galaxy population.

2 COSMOLOGY AND STRUCTURE FORMATION

2.1 Dark energy cosmologies

In a spatially flat dark energy cosmology with a constant dark energy equation of state parameter w, the Hubble function $H(a) = \mathrm{d}\ln a/\mathrm{d}t$ is given by

$$\frac{H^2(a)}{H_0^2} = \frac{\Omega_m}{a^3} + \frac{1-\Omega_m}{a^{3(1+w)}}. \tag{1}$$

The conformal time follows directly from the definition of the Hubble function,

$$\eta = \int_a^1 \mathrm{d}a\,\frac{1}{a^2 H(a)}, \tag{2}$$

in units of the Hubble time $t_H = 1/H_0$. Correspondingly, the definition of the comoving distance χ is given by $\chi = c\eta$ with the speed of light c.

2.2 CDM power spectrum

A common parametrization for the CDM power spectrum is $P(k) \propto k^{n_s} T^2(k)$ for describing the Gaussian fluctuation statistics of the homogeneous and isotropic cosmic density field δ,

$$\langle \delta(\boldsymbol{k})\delta(\boldsymbol{k}')^* \rangle = (2\pi)^3 \delta_D(\boldsymbol{k}-\boldsymbol{k}') P(k). \tag{3}$$

According to Bardeen et al. (1986), a convenient fit to the CDM transfer function $T(k)$ is

$$T(q) = \frac{\ln(1 + 2.34q)}{2.34q}$$
$$\times [1 + 3.89q + (16.1q)^2 + (5.46q)^3 + (6.71q)^4]^{-1/4},$$

where the wavevector q is given in units of the shape parameter $\Gamma \simeq \Omega_m h$. $P(k)$ is normalized to the value σ_8 on the scale $R = 8\,\mathrm{Mpc}\,h^{-1}$,

$$\sigma_R^2 = \frac{1}{2\pi^2} \int \mathrm{d}k\, k^2 W^2(kR) P(k), \tag{4}$$

with a Fourier-transformed spherical top hat $W(x) = 3j_1(x)/x$ as the filter function. $j_\ell(x)$ denotes the spherical Bessel function of the first kind of order ℓ (Abramowitz & Stegun 1972). Smith et al. (2009) found that non-linear effects in the biasing model amount to $\sim$10 per cent, but for simplicity, we assume a linear, local, non-evolving and scale-independent biasing scheme,

$$\frac{\Delta n}{n} = \frac{\Delta \rho}{\rho}, \tag{5}$$

and relate fluctuations Δn in the spatial number density n of galaxies directly to the dark matter overdensity $\delta = \Delta\rho/\rho$.

2.3 Structure growth in dark energy cosmologies

The linearized structure formation equations can be combined to the growth equation (Turner & White 1997; Wang & Steinhardt 1998; Linder & Jenkins 2003),

$$\frac{\mathrm{d}^2}{\mathrm{d}a^2}D_+ + \frac{1}{a}\left(3 + \frac{\mathrm{d}\ln H}{\mathrm{d}\ln a}\right)\frac{\mathrm{d}}{\mathrm{d}a}D_+ = \frac{3}{2a^2}\Omega_m(a)D_+(a), \tag{6}$$

whose solution $D_+(a)$ describes the homogeneous growth of the density field, $\delta(\boldsymbol{x}, a) = D_+(a)\delta(\boldsymbol{x}, 1)$.

3 OBSERVABLES: iSW EFFECT AND TRACERS

3.1 iSW temperature perturbation

The iSW effect is caused by gravitational interactions of CMB photons with time-evolving potentials Φ. The fractional perturbation τ of the CMB temperature T_{CMB} is given by (Sachs & Wolfe 1967; Rees & Sciama 1968)

$$\tau = \frac{\Delta T}{T_{CMB}} = -\frac{2}{c^3}\int_0^{\chi_H} \mathrm{d}\chi\, a^2 H(a)\frac{\partial\Phi}{\partial a}. \tag{7}$$

The gravitational potential Φ is a solution to the comoving Poisson equation,

$$\Delta\Phi = \frac{3H_0^2\Omega_m}{2a}\delta. \tag{8}$$

Substituting into the line-of-sight expression for the linear iSW effect τ (integrating along a straight line and using the flat-sky approximation) yields

$$\tau = \frac{3\Omega_m}{c}\int_0^{\chi_H} \mathrm{d}\chi\, a^2 H(a)\frac{\mathrm{d}}{\mathrm{d}a}\left(\frac{D_+}{a}\right)\frac{\Delta^{-1}}{\chi_H^2}\delta, \tag{9}$$

where the inverse Laplace operator Δ^{-1}/χ_H^2 solves for the potential

$$\varphi \equiv \frac{\Delta^{-1}}{\chi_H^2}\delta. \tag{10}$$

The square of the Hubble distance $\chi_H = c/H_0$ makes the differential operator dimensionless.

3.2 Galaxy density as a large-scale structure tracer

The projected galaxy density γ can be related to the CDM density δ via

$$\gamma = \int_0^{\chi_H} \mathrm{d}\chi\, p(z)\frac{\mathrm{d}z}{\mathrm{d}\chi}D_+(\chi)\,\delta, \tag{11}$$

where $p(z)\,\mathrm{d}z$ is the redshift distribution of the surveyed galaxy sample, rewritten in terms of the comoving distance χ. We use the main galaxy sample of *Euclid* which will survey a fraction $f_{sky} =$

0.5 of the sky with a median redshift of $z_{med} = 0.9$ (Douspis et al. 2008). We use the parametrization proposed by Smail et al. (1995):

$$p(z)\,\mathrm{d}z = p_0\left(\frac{z}{z_0}\right)^2 \exp\left(-\left(\frac{z}{z_0}\right)^\beta\right)\mathrm{d}z \quad \text{with} \quad \frac{1}{p_0} = \frac{z_0}{\beta}\Gamma\left(\frac{3}{\beta}\right),$$
(12)

for $p(z)\,\mathrm{d}z$, with $z_0 = 0.64$. We assume a constant bias of $b = 1$, which we absorb into the normalization σ_8 of the power spectra.

4 PERTURBATIVE CORRECTIONS

For a consistent derivation of the iSW spectrum including corrections due to the non-linearly evolved source fields one needs to carry out a perturbative expansion to third order,

$$\delta(\boldsymbol{x}, a) \simeq \sum_{n=1}^{3} D_+^n(a)\delta^{(n)}(\boldsymbol{x}) + \mathcal{O}(\delta^4).$$
(13)

The linearity of the Poisson equation conserves the perturbative series,

$$\dot{\varphi}(\boldsymbol{x}, a) \simeq \sum_{n=1}^{3} \frac{\mathrm{d}}{\mathrm{d}a}\frac{D_+^n}{a}\varphi^{(n)} + \mathcal{O}(\varphi^4),$$
(14)

and suggests that the time derivative of the potential is $\propto \mathrm{d}(D_+^n/a)/\mathrm{d}a$. In perturbation theory, the second- and third-order corrections to the density field are given by

$$\delta^{(2)}(\boldsymbol{k}) = \int \frac{\mathrm{d}^3 p}{(2\pi)^3}\, M_2(\boldsymbol{k} - \boldsymbol{p}, \boldsymbol{p})\delta(\boldsymbol{p})\delta(|\boldsymbol{k} - \boldsymbol{p}|),$$
(15)

$$\delta^{(3)}(\boldsymbol{k}) = \int \frac{\mathrm{d}^3 p}{(2\pi)^3}$$
$$\times \int \frac{\mathrm{d}^3 q}{(2\pi)^3}\, M_3(\boldsymbol{p}, \boldsymbol{q}, \boldsymbol{k} - \boldsymbol{p} - \boldsymbol{q})\delta(\boldsymbol{p})\delta(\boldsymbol{q})\delta(|\boldsymbol{k} - \boldsymbol{p} - \boldsymbol{q}|),$$
(16)

where the mode-coupling functions $M_2(\boldsymbol{p}, \boldsymbol{q})$ and $M_3(\boldsymbol{p}, \boldsymbol{q}, \boldsymbol{r})$ (see Sahni & Coles 1995; Bernardeau et al. 2002) are a consequence of the inhomogeneous growth and introduce non-Gaussianities in the evolved density field. The power spectrum $P_{\delta\delta}^{(11)}(k) = P(k)$ of the density field thus acquires the corrections

$$P_{\delta\delta}^{(22)}(k) = 2\int \frac{\mathrm{d}^3 p}{(2\pi)^3}\, M_2(\boldsymbol{k} - \boldsymbol{p}, \boldsymbol{p})^2 P(|\boldsymbol{k} - \boldsymbol{p}|)P(|\boldsymbol{p}|),$$
(17)

$$P_{\delta\delta}^{(13)}(k) = 3\int \frac{\mathrm{d}^3 p}{(2\pi)^3}\, M_3(\boldsymbol{k}, \boldsymbol{p}, -\boldsymbol{p})P(k)P(|\boldsymbol{p}|).$$
(18)

In the computation of these corrections, the cylindrical symmetry of the kernels M_2 and M_3 can be taken advantage of, reducing to a two-fold integration $2\pi p^2 \mathrm{d}p\mathrm{d}\mu$ with μ being the cosine of the angle between $\boldsymbol{k}$ and $\boldsymbol{p}$. In perturbation theory, the contribution $P_{\delta\delta}^{12}(k)$ is reduced to the third-order moment of the initial Gaussian density field and drops out, likewise, the contribution $P_{\delta\delta}^{(23)}(k)$.

Fig. 1 shows the time evolution of the source fields, i.e. the growth function $D_+^n(a)$ for the density field and the time derivative of $D_+^n(a)/a$ for the iSW source field, both up to perturbative order $n = 3$. While the growth functions show a similar behaviour in higher order, the derivatives are qualitatively very different. The evaluations of the integrals are done in a coordinate system whose p_z-axis is parallel to k_z. The non-linear corrections to the CDM spectrum $P(k)$ are shown in Fig. A1.

An interesting peculiarity of the non-linear RS effect in comparison to the linear iSW effect is worth mentioning: whereas in SCDM
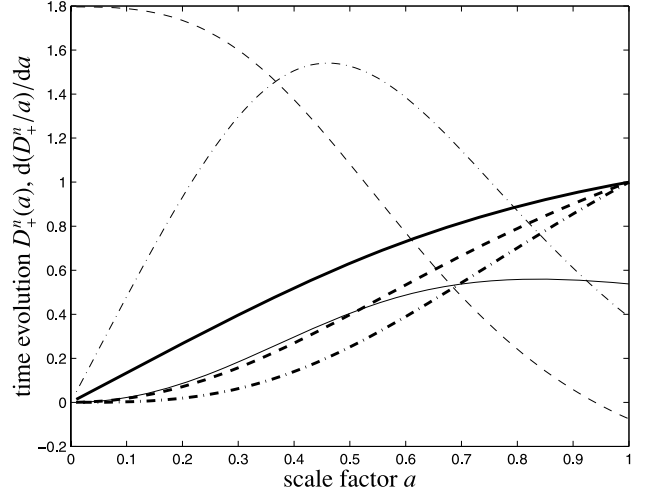

Figure 1. Time evolution of the source term $D_+^n(a)$ for the density field (thick line) and the modulus of $\mathrm{d}(D_+^n/a)/\mathrm{d}a$ for the iSW effect (thin line), for the linear order $n = 1$ (solid line) and the non-linear corrections $n = 2$ (dashed line) and $n = 3$ (dash–dotted line), with ΛCDM as the cosmological model.

cosmologies the iSW effect vanishes due to $D_+(a) \equiv a$ and is non-zero in dark energy cosmologies, the RS effect is the strongest in SCDM and weaker in dark energy cosmologies, at least at the low redshifts we observe, where $D_+(a) \simeq a^\alpha$ with $\alpha < 1$. Applying a simple scaling argument by only looking at the pre-factors, the cross-spectra of the RS effect are proportional to $\Omega_m\sigma_8^4$ (up to third order in perturbation theory), in contrast to the iSW spectrum, which scales as $\Omega_m\sigma_8^2$. As will be shown in Figs 2 and 3, the dependence on the dark energy equation of state parameter w is weaker in the non-linear effect and the shape of the spectrum (determined by h and n_s) becomes less important because of the integrations over $\mathrm{d}^3 p$ carried out in perturbation theory. These arguments motivate the quantification of the RS contamination of the iSW spectrum, and their interference with the estimation of cosmological parameters.
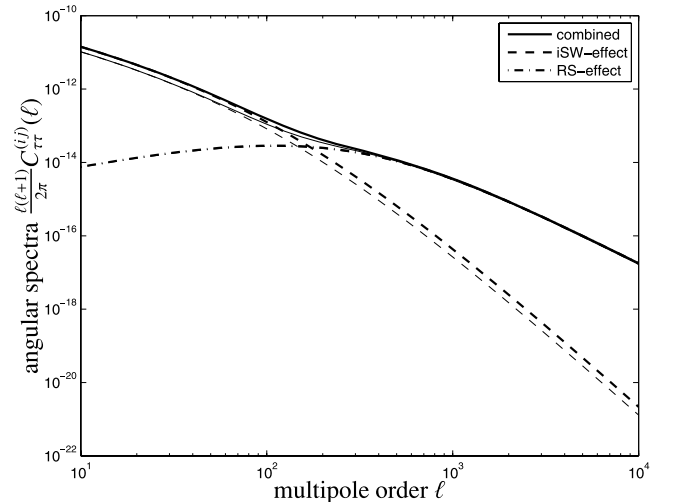

Figure 2. Angular iSW-spectrum $C_{\tau\tau}(\ell)$ of the iSW-effect (solid line), split up into the linear effect $C_{\tau\tau}^{(11)}(\ell)$ (dashed line) and the non-linear RS corrections $C_{\tau\tau}^{(22)}(\ell) + C_{\tau\tau}^{(13)}(\ell)$ (dashed–dotted line). The plot compares spectra for wCDM with $w = -0.9$ (thick lines) with ΛCDM with $w = -1$ (thin lines).
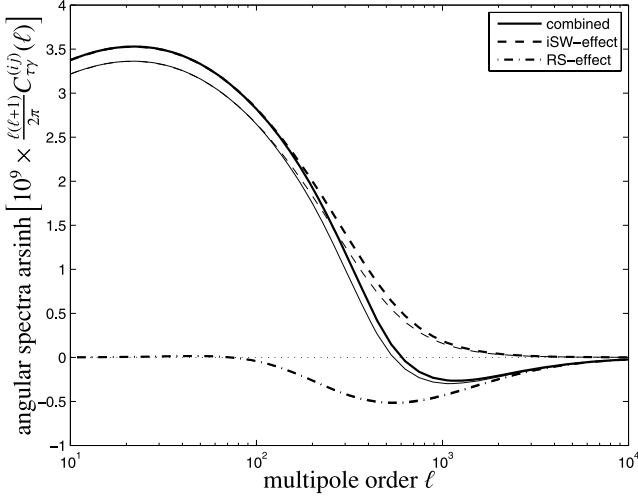
Figure 3. Angular iSW cross-spectrum $C_{\tau\gamma}(\ell)$ of the iSW effect (solid line), split up into the linear effect $C_{\tau\gamma}^{(11)}(\ell)$ (dashed line) and the non-linear RS corrections $C_{\tau\gamma}^{(22)}(\ell) + C_{\tau\gamma}^{(13)}(\ell)$ (dashed–dotted line), both for wCDM ($w = -0.9$, thick lines) and ΛCDM ($w = -1$, thin lines).

5 ANGULAR POWER SPECTRA

In summary, the line-of-sight integrals for the iSW temperature perturbation $\tau^{(n)}$ and the galaxy density $\gamma^{(n)}$ in order n read

$$\tau^{(n)} = \frac{3\Omega_m}{c} \int_0^{\chi_H} d\chi \, a^2 H(a) \frac{d}{da}\left(\frac{D_+^n}{a}\right) \varphi^{(n)}, \tag{19}$$

$$\gamma^{(n)} = \int_0^{\chi_H} d\chi \, p(z) \frac{dz}{d\chi} D_+^n(\chi) \delta^{(n)}, \tag{20}$$

where we have defined the dimensionless potential $\varphi^{(n)} \equiv \Delta^{-1}\delta^{(n)}/\chi_H^2$ from the inversion of the Poisson equation, rescaled with the square of the Hubble distance $\chi_H = c/H_0$ for convenience. Due to the linearity of the Newtonian Poisson relation, the perturbative corrections in δ map directly on to the corrections in φ. The weighting functions,

$$W_\tau^{(n)}(\chi) = \frac{3\Omega_m}{c} a^2 H(a) \frac{d}{da} \frac{D_+^n}{a}, \tag{21}$$

$$W_\gamma^{(n)}(\chi) = p(z) \frac{dz}{d\chi} D_+^n(\chi), \tag{22}$$

can be identified, which allow the expressions for the angular cross-spectra to be written in a compact notation, applying a Limber projection (Limber 1954) in the flat-sky approximation:

$$C_{\tau\gamma}^{(11)}(\ell) = \int_0^{\chi_H} \frac{d\chi}{\chi^2} W_\tau^{(1)}(\chi) W_\gamma^{(1)}(\chi) P_{\delta\varphi}^{(11)}(\ell/\chi), \tag{23}$$

$$C_{\tau\gamma}^{(13)}(\ell) = \int_0^{\chi_H} \frac{d\chi}{\chi^2} \left(W_\tau^{(1)}(\chi) W_\gamma^{(3)}(\chi) + W_\tau^{(3)}(\chi) W_\gamma^{(1)}(\chi)\right) P_{\delta\varphi}^{(13)}(\ell/\chi), \tag{24}$$

$$C_{\tau\gamma}^{(22)}(\ell) = \int_0^{\chi_H} \frac{d\chi}{\chi^2} W_\tau^{(2)}(\chi) W_\gamma^{(2)}(\chi) P_{\delta\varphi}^{(22)}(\ell/\chi), \tag{25}$$

with the cross-spectrum $P_{\delta\varphi}^{(ij)}(k) = P_{\delta\delta}^{(ij)}(k)/(\chi_H k)^2$. The expression for the spectrum $C_{\tau\gamma}^{(13)}(\ell)$ has been symmetrized. The angular autospectra of the temperature perturbation τ are given by

$$C_{\tau\tau}^{(11)}(\ell) = \int_0^{\chi_H} \frac{d\chi}{\chi^2} W_\tau^{(1)}(\chi)^2 P_{\varphi\varphi}^{(11)}(\ell/\chi), \tag{26}$$

$$C_{\tau\tau}^{(13)}(\ell) = 2 \int_0^{\chi_H} \frac{d\chi}{\chi^2} W_\tau^{(1)}(\chi) W_\tau^{(3)}(\chi) P_{\varphi\varphi}^{(13)}(\ell/\chi), \tag{27}$$

$$C_{\tau\tau}^{(22)}(\ell) = \int_0^{\chi_H} \frac{d\chi}{\chi^2} W_\tau^{(2)}(\chi)^2 P_{\varphi\varphi}^{(22)}(\ell/\chi). \tag{28}$$

In analogy to $P_{\delta\varphi}^{(ij)}(k)$, the spectrum of the potential φ is defined as $P_{\varphi\varphi}^{(ij)}(k) = P_{\delta\delta}^{(ij)}(k)/(\chi_H k)^4$. Finally, the spectra of the galaxy density γ can be evaluated to be

$$C_{\gamma\gamma}^{(11)}(\ell) = \int_0^{\chi_H} \frac{d\chi}{\chi^2} W_\gamma^{(1)}(\chi)^2 P_{\delta\delta}^{(11)}(\ell/\chi), \tag{29}$$

$$C_{\gamma\gamma}^{(13)}(\ell) = 2 \int_0^{\chi_H} \frac{d\chi}{\chi^2} W_\gamma^{(1)}(\chi) W_\gamma^{(3)}(\chi) P_{\delta\delta}^{(13)}(\ell/\chi), \tag{30}$$

$$C_{\gamma\gamma}^{(22)}(\ell) = \int_0^{\chi_H} \frac{d\chi}{\chi^2} W_\gamma^{(2)}(\chi)^2 P_{\delta\delta}^{(22)}(\ell/\chi). \tag{31}$$

Collecting all terms, the full spectra consist of one first-order and two second-order contributions:

$$C_{\tau\gamma}(\ell) = C_{\tau\gamma}^{(11)}(\ell) + C_{\tau\gamma}^{(22)}(\ell) + C_{\tau\gamma}^{(13)}(\ell), \tag{32}$$

$$C_{\tau\tau}(\ell) = C_{\tau\tau}^{(11)}(\ell) + C_{\tau\tau}^{(22)}(\ell) + C_{\tau\tau}^{(13)}(\ell), \tag{33}$$

$$C_{\gamma\gamma}(\ell) = C_{\gamma\gamma}^{(11)}(\ell) + C_{\gamma\gamma}^{(22)}(\ell) + C_{\gamma\gamma}^{(13)}(\ell). \tag{34}$$

Because of the linearity of equations (19) and (20) all correlation functions of the source field map on to their corresponding angular correlation functions and the vanishing $P_{\delta\delta}^{(12)}(k)$ contribution is not able to generate an angular spectrum.

Figs 2 and 3 give the iSW autospectra and cross-spectra, respectively, split up into linear contributions and the two perturbative corrections. The iSW autospectrum is dominated on multipoles larger than 100 and the cross-spectrum is suppressed by the negative correlation between iSW effect and tracer density on similar scales, leading to a sign change of the cross-spectrum at $\ell \simeq 500$, which confirms earlier perturbative and N-body results (Seljak 1996; Cooray 2002; Cai et al. 2008; Nishizawa et al. 2008; Smith et al. 2009), but using a different perturbation theory approach. arsinh(x) is equal to x for $|x| \ll 1$ and $\propto \ln x$ for $|x| \gg 1$, which allows us to show the logarithmic behaviour of $C_{\tau\gamma}(\ell)$ despite the sign change. Another interesting feature is the fact that the non-linear effect is much less sensitive on the properties of dark energy, in particular the dark energy equation of state parameter w, for which the RS spectra depicted differ by about 5 per cent. The sign change and its sensitivity on w is mostly driven by changes in $C_{\tau\gamma}^{(11)}(\ell)$. Fig. A2 gives the cross-spectrum in a logarithmic representation and shows that the anticorrelation between τ and γ is a generic feature of non-linearly evolving structures from angular scales of $\ell \simeq 70$ on, but the linear effect shifts the anticorrelation scales to much higher multipole moments. The sign change can be easily explained by the fact that in linear structure formation potentials are constant or decay slowly, depending on cosmology, whereas in non-linear structure formation the potentials grow fast, which manifest itself in the iSW effect by causing temperature perturbations of opposite sign.

6 STATISTICAL ERRORS

In this chapter, we recapitulate the estimation of statistical precision on parameters derived from angular iSW spectra with Fisher matrices (Tegmark, Taylor & Heavens 1997), and the accuracy of the parameter estimation with an extended Fisher formalism (Amara & Refregier 2007; Cabré et al. 2007; Taburet et al. 2009).

6.1 Fisher matrix for the iSW spectrum $C_{\tau\gamma}(\ell)$

The Fisher matrix, which quantifies the decrease in likelihood if a model parameter x_μ moves away from the fiducial value, can be computed for a local Gaussian approximation to likelihood $\mathcal{L} \propto \exp(-\chi^2/2)$. The Fisher matrix for the measurement of $C_{\tau\gamma}(\ell)$ is given by

$$F_{\mu\nu}^{\text{iSW}} = \sum_{\ell=\ell_{\min}}^{\ell_{\max}} \frac{\partial C_{\tau\gamma}(\ell)}{\partial x_\mu} \text{Cov}^{-1}\left(C_{\tau\gamma}(\ell), C_{\tau\gamma}(\ell)\right) \frac{\partial C_{\tau\gamma}(\ell)}{\partial x_\nu}. \tag{35}$$

We construct the Fisher matrix $F_{\mu\nu}$ for ΛCDM as the fiducial cosmological model, with fiducial values for the parameters being $\Omega_m = 0.25$, $\sigma_8 = 0.8$, $h = 0.72$, $n_s = 1$ and $w = -1$. Implicitly, we assume priors on spatial flatness, $\Omega_m + \Omega_\Lambda = 1$ and neglect the weak dependence of the shape parameter on the baryon density Ω_b. CMB priors on the cosmological parameters are incorporated by adding the CMB Fisher matrix $F_{\mu\nu}^{\text{CMB}}$:

$$F_{\mu\nu} = F_{\mu\nu}^{\text{iSW}} + F_{\mu\nu}^{\text{CMB}}, \tag{36}$$

which is valid if $C_{\tau\gamma}(l)^2 \ll C_{\tau\tau}(\ell)C_{\gamma\gamma}(\ell)$, adapting the results of Ho et al. (2008). For the iSW spectrum in a ΛCDM cosmology, it can be shown that the ratio $C_{\tau\gamma}/\sqrt{C_{\tau\tau}C_{\gamma\gamma}}$ for the iSW effect alone would be close to 1, dropping to values of 0.1 at larger multipoles, but the inclusion of instrumental noise and primary CMB fluctuations shifts the ratio to values close to zero, such that the assumption of approximately independent likelihoods is justified.

6.2 Noise modelling

In an actual observation, the iSW power spectrum is modified by the intrinsic CMB fluctuations, the instrumental noise and the beam as noise sources, assuming mutual uncorrelatedness of the individual contributions. The galaxy correlation function assumes a Poissonian noise term,

$$\tilde{C}_{\tau\tau}(\ell) = C_{\tau\tau}(\ell) + C_{\text{CMB}}(\ell) + w_T^{-1}B^{-2}(\ell), \tag{37}$$

$$\tilde{C}_{\gamma\gamma}(\ell) = C_{\gamma\gamma}(\ell) + \frac{1}{n}. \tag{38}$$

For *Planck*'s noise levels the value $w_T^{-1} = (0.02\,\mu\text{K})^2$ has been used, and the beam was assumed to be Gaussian, $B^{-2}(\ell) = \exp(\Delta\theta^2\,\ell(\ell+1))$, with a full width at half-maximum (FWHM) of $\Delta\theta = 7.1$ arcmin, corresponding to channels of *Planck* closest to the CMB maximum at $\simeq 160$ GHz (Knox 1995; Douspis et al. 2008).

Euclid is designed to survey the entire extragalactic sky and to cover the solid angle $\Delta\Omega = 2\pi$, corresponding to $f_{\text{sky}} = 0.5$, yielding a total of $n = 4.7 \times 10^8$ galaxies per steradian at a density of 40 galaxies arcmin^{-2} (Amara & Réfrégier 2007; Refregier et al. 2009). The observed cross-power spectra are unbiased estimates of the actual spectra,

$$\tilde{C}_{\tau\gamma}(\ell) = C_{\tau\gamma}(\ell), \tag{39}$$

in the case of uncorrelated noise terms. We determine the spectrum $C_{\text{CMB}}(\ell)$ of the primary CMB anisotropies with the CAMB code

(Lewis, Challinor & Lasenby 2000). The covariance of the spectrum $C_{\tau\gamma}(\ell)$ is given in terms of the observed spectra $\tilde{C}_{\tau\tau}(\ell)$, $\tilde{C}_{\tau\gamma}(\ell)$ and $\tilde{C}_{\gamma\gamma}(\ell)$ which follow directly from applying the Wick theorem,

$$\text{Cov}(C_{\tau\gamma}, C_{\tau\gamma}) = \frac{1}{2\ell+1}\frac{1}{f_{\text{sky}}}\left[\tilde{C}_{\tau\gamma}^2(\ell) + \tilde{C}_{\tau\tau}(\ell)\tilde{C}_{\gamma\gamma}(\ell)\right]. \tag{40}$$

In all applications considered in this paper, *Planck* causes the dominating noise contribution in comparison to the Poisson noise in the galaxy number density given by *Euclid*.

6.3 Detectability of the RS effect

The signal-to-noise ratio Σ of the cross-spectrum $C_{\tau\gamma}(\ell)$ reads

$$\Sigma^2 = \sum_{\ell=\ell_{\min}}^{\ell_{\max}} \frac{C_{\tau\gamma}^2(\ell)}{\text{Cov}(C_{\tau\gamma}(\ell))}, \tag{41}$$

for mutually uncorrelated modes as in the case of a full-sky observation. Fig. 4 shows the signal-to-noise ratio Σ of a measurement of $C_{\tau\gamma}(\ell)$ including the non-linear contribution at high ℓ. The figure suggests that ideal cosmic variance limited experiments can in fact detect the RS effect with a significance of 3.22σ (corresponding to a confidence of 0.998) integrating over all multipoles up to $\ell = 3 \times 10^3$, and that this significance is reduced by the finite resolution and the noise of *Planck* to a mere 0.77σ (0.558 confidence). Thus, the signal-to-noise ratio of the non-linear effect is roughly smaller by an order of magnitude compared to that of the linear iSW effect. Apart from the increasing correlation noise at high ℓ, it is the smallness of the spectrum around the cross-over scale which does not provide enough signal for a detection. Between $\ell = 30$ and 100 the cumulative signal-to-noise ratio stagnates, which is not included in the computation by Cooray (2002) as his perturbative approach is not able to reproduce the small values of $d\Sigma/dl$ due to the sign change of $C_{\tau\gamma}(\ell)$ at $\ell \simeq 70$. Despite the sensitivity of the cross-over scale on e.g. the dark energy equation of state parameter w it would be very difficult to measure this scale as the signal-to-noise ratio of each multipole is about 10^{-3} and as the same knowledge on w can be already derived from much smaller multipoles with sufficient
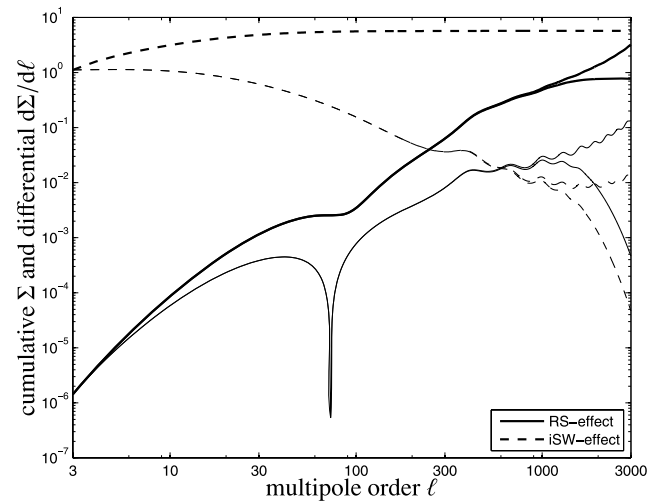

Figure 4. Signal-to-noise ratio of a measurement of the cross-spectrum $C_{\tau\gamma}(\ell)$, cumulative Σ (thick lines) and differential $d\Sigma/d\ell$ (thin lines), for the linear iSW effect (dashed line) and the non-linear RS effect (solid line). The plot compares the signal-to-noise ratio attainable with hypothetical cosmic variance limited experiments (upper set of lines) with that reachable by combining *Planck* with *Euclid* (lower set of lines).

accuracy. The non-zero instrumental noise (the shot noise in the galaxy density and the *Planck* noise) causes the graphs for Σ and $d\Sigma/d\ell$ to branch in the vicinity of $\ell = 1000$, where the cumulative signal-to-noise ratio Σ levels off and the contribution per multipole $d\Sigma/d\ell$ drops rapidly for a noisy experiment in comparison to ideal, noise-free experiments only limited by cosmic variance. The wiggles in the graphs for $d\Sigma/d\ell$ are acoustic features in the CMB which enter through the covariance.

6.4 Parameter bounds and degeneracies

The χ^2 function for a pair of parameters (x_μ, x_ν) can be computed from the inverse $(F^{-1})_{\mu\nu}$ of the Fisher matrix

$$\chi^2 = \begin{pmatrix} \Delta x_\mu \\ \Delta x_\nu \end{pmatrix}^t \begin{pmatrix} (F^{-1})_{\mu\mu} & (F^{-1})_{\mu\nu} \\ (F^{-1})_{\nu\mu} & (F^{-1})_{\nu\nu} \end{pmatrix}^{-1} \begin{pmatrix} \Delta x_\mu \\ \Delta x_\nu \end{pmatrix}, \tag{42}$$

where $\Delta x_\mu = x_\mu - x_\mu^{\Lambda\mathrm{CDM}}$. The correlation coefficient $r_{\mu\nu}$ is defined as

$$r_{\mu\nu} = \frac{(F^{-1})_{\mu\nu}}{\sqrt{(F^{-1})_{\mu\mu}(F^{-1})_{\nu\nu}}}, \tag{43}$$

and describes the degree of dependence between the parameters x_μ and x_ν by assuming numerical values close to 0 for independent parameters and close to unity for strongly dependent parameters. The degeneracies between the cosmological parameters Ω_m, σ_8, h, n_s and w estimated from the linear iSW effect is shown in Fig. 5,

along with the correlation coefficient from a measurement combining *Planck* and *Euclid* data up to very high multipoles of $\ell = 3000$, including a prior from CMB data.

7 SYSTEMATICAL ERRORS

In this section, we quantify how the interpretation of the data with the pure iSW spectrum affects the estimation of cosmological parameters, if in reality there are non-linear RS contributions at higher multipoles. Using this formalism, we seek to minimize the combined statistical error by finding an optimal angular scale ℓ_opt down to which the iSW measurement should be carried out. The non-linear iSW effect is the dominant contamination of the iSW spectrum at intermediate multipoles, with the kinetic Sunyaev–Zel'dovich effect becoming important at multipoles above $\ell \simeq 10^3$. The parameter estimation bias formalism has been validated with Monte Carlo Markov chains and was found to be an excellent approximation for weak systematics (Taburet, Douspis & Aghanim 2010).

7.1 Estimation bias formalism

The angular iSW spectrum $C_{\tau\gamma}(\ell) = C_\mathrm{iSW}(\ell) + C_\mathrm{RS}(\ell)$ can be separated into the linear part $C_\mathrm{iSW}(\ell)$ and an additive systematic $C_\mathrm{RS}(\ell)$ due to the non-linear corrections,

$$C_\mathrm{iSW}(\ell) = C_{\tau\gamma}^{(11)}(\ell), \tag{44}$$

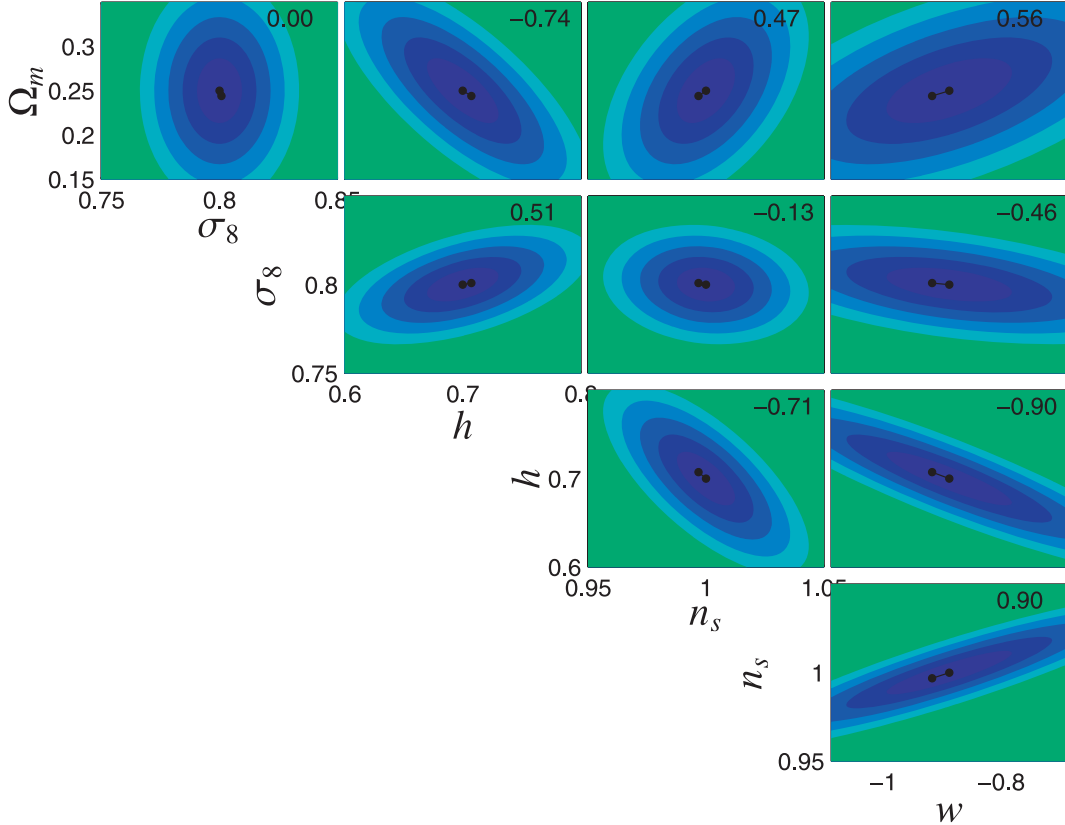$$C_\mathrm{RS}(\ell) = C_{\tau\gamma}^{(22)}(\ell) + C_{\tau\gamma}^{(13)}(\ell). \tag{45}$$

Figure 5. Constraints on the parameters Ω_m, σ_8, n_s, h and w from the cross-correlation of *Planck* with *Euclid*. The ellipses correspond to 1σ–5σ confidence regions. Additionally, the vectors (δ_μ, δ_ν) indicate the bias in the estimation of the cosmological parameters due to the non-linear contributions and have been *enlarged by a factor of 10*. The estimation bias was derived for a multipole range extending up to $\ell_\mathrm{max} = 3 \times 10^3$. The number in the upper right-hand corner of each panel gives the correlation coefficient $r_{\mu\nu}$. The constraints include a prior from the statistics $C_\mathrm{CMB}(\ell)$ of primary CMB temperature anisotropies on both the statistical and systematical error.

Using these relations, we define the power spectrum of the true model $C_t(\ell)$ including non-linear corrections,

$$C_t(\ell) = C_{\mathrm{iSW}}(\ell) + C_{\mathrm{RS}}(\ell) = C_{\tau\gamma}^{(11)}(\ell) + C_{\tau\gamma}^{(22)}(\ell) + C_{\tau\gamma}^{(13)}(\ell), \quad (46)$$

as well as the spectrum of the false model $C_f(\ell)$, which neglects these RS contributions,

$$C_f(\ell) = C_{\mathrm{iSW}}(\ell) = C_{\tau\gamma}^{(11)}(\ell), \quad (47)$$

where the observed spectra $\tilde{C}_i(\ell)$ are unbiased estimators of the theoretical spectra $C_i(\ell)$ in each case because of uncorrelated errors in each observational channel in the cross-correlation measurement method. The estimation of cosmological parameters is carried out from maximization of the χ^2 functionals of the two competing models,

$$\chi_t^2 = \sum_{\ell=\ell_{\min}}^{\ell_{\max}} \frac{(\tilde{C}_t(\ell) - C_t(\ell))^2}{\mathrm{Cov}\,[C_t(\ell), C_t(\ell)]} \quad (48)$$

and

$$\chi_f^2 = \sum_{\ell=\ell_{\min}}^{\ell_{\max}} \frac{(\tilde{C}_t(\ell) - C_f(\ell))^2}{\mathrm{Cov}[C_f(\ell), C_f(\ell)]}, \quad (49)$$

i.e. the data are in reality described by $C_t(\ell)$ and, in the second case, fitted wrongly with $C_f(\ell)$ instead of $C_t(\ell)$. The best-fitting parameters $\boldsymbol{x}$ for each model can be derived by solving the equations $\langle \partial \chi^2 / \partial x_\mu \rangle = 0$ following from the respective χ^2 functional.

For deriving the distance $\boldsymbol{x}_f - \boldsymbol{x}_t$ between the best-fitting values of the true and the false models, we expand the χ_f^2 function at the best-fitting position $\boldsymbol{x}_t$ in a Taylor series (see Taburet et al. 2009)

$$\chi_f^2(\boldsymbol{x}_f) = \chi_f^2(\boldsymbol{x}_t) + \sum_\mu \frac{\partial}{\partial x_\mu} \chi_f^2(\boldsymbol{x}_t)\, \delta_\mu$$
$$+ \frac{1}{2} \sum_{\mu,\nu} \frac{\partial^2}{\partial x_\mu \partial x_\nu} \chi_f^2(\boldsymbol{x}_t)\, \delta_\mu \delta_\nu, \quad (50)$$

where the parameter estimation bias vector $\delta \equiv \boldsymbol{x}_f - \boldsymbol{x}_t$ was defined. The best-fitting position $\boldsymbol{x}_f$ of χ_f^2 can be recovered by extremization of the ensemble-averaged $\langle \chi_f^2 \rangle$, yielding

$$\left\langle \frac{\partial}{\partial x_\mu} \chi_f^2 \right\rangle_{\boldsymbol{x}_t} = -\sum_\nu \left\langle \frac{\partial^2}{\partial x_\mu \partial x_\nu} \chi_f^2 \right\rangle_{\boldsymbol{x}_t} \delta_\nu, \quad (51)$$

which is a linear system of equations of the form

$$\sum_\nu G_{\mu\nu} \delta_\nu = a_\mu \rightarrow \delta_\mu = \sum_\nu (G^{-1})_{\mu\nu} a_\nu, \quad (52)$$

where the two quantities $G_{\mu\nu}$ and a_μ follow from the derivatives of the χ_f^2 function, evaluated at $\boldsymbol{x}_t$,

$$G_{\mu\nu}^{\mathrm{iSW}} \equiv \sum_{\ell=\ell_{\min}}^{\ell_{\max}} \mathrm{Cov}^{-1} \left[\frac{\partial C_{\mathrm{iSW}}(\ell)}{\partial x_\mu} \frac{\partial C_{\mathrm{iSW}}(\ell)}{\partial x_\nu} - C_{\mathrm{RS}}(\ell) \frac{\partial^2 C_{\mathrm{iSW}}(\ell)}{\partial x_\mu \partial x_\nu} \right], \quad (53)$$

$$a_\mu \equiv \sum_{\ell=\ell_{\min}}^{\ell_{\max}} \mathrm{Cov}^{-1} \left[C_{\mathrm{RS}}(\ell) \frac{\partial C_{\mathrm{iSW}}(\ell)}{\partial x_\mu} \right].$$

The CMB priors can be incorporated by adding the Fisher matrix $F_{\mu\nu}^{\mathrm{CMB}}$ to $G_{\mu\nu}$,

$$G_{\mu\nu} = G_{\mu\nu}^{\mathrm{iSW}} + F_{\mu\nu}^{\mathrm{CMB}}, \quad (54)$$

for independent iSW and CMB likelihoods. In this formalism, it is quite natural that one observes large parameter shifts in weakly constrained parameters, which is a consequence of the relation between $F_{\mu\nu}$ and $G_{\mu\nu}$: if the systematic vanishes, the two are identical. A

nice example is the sensitivity of the iSW effect on the parameters w and σ, which both change the amplitude of the spectrum, with σ_8 having a stronger effect. If the amplitude of the iSW spectrum is increased due to a present RS systematic, the data can be explained by larger parameter values where the parameter to which the iSW spectrum is less sensitive needs to be detuned more. Therefore, one can expect larger systematics in the more weakly constrained parameter, i.e. there will be more estimation bias in w compared to σ_8. Of course this argument is only valid for parameter pairs that are degenerate in explaining features of the measured spectrum.

The biases in parameter estimation from the iSW effect are depicted alongside the degeneracies in Fig. 5, for a maximum multipole order of $\ell_{\max} = 3000$. The parameter estimation biases in the combined set of cosmological parameters are very small due to the weakness of the RS signal in comparison to that of the iSW effect and due to the strong prior from primary CMB fluctuations. Typical values for misestimates in cosmological parameters are of the order of $<0.1\sigma$, and are negligible in comparison to statistical errors.

7.2 Contamination of the iSW spectrum

In this section, we consider the application of the iSW effect for providing independent constraints on individual cosmological parameters. If the iSW likelihood is combined with the CMB likelihood according to equation (54), the latter is by far dominating due to larger signal-to-noise ratio. Although the signal strength of the iSW effect is not enough for fully constraining a standard dark energy cosmology with five or more parameters, it is sufficient to place competitive bounds on single cosmological parameters. Therefore, we define the conditional systematical error $\sigma_\mu = 1/\sqrt{F_{\mu\mu}}$ and the systematical error b_μ on a single parameter x_μ while all other parameters are assumed to coincide exactly with their fiducial values.

At low multipoles, the error budget will be dominated by statistics, while the systematics due to the non-linear contributions are negligible . Conversely, the extension of the computation to higher multipoles $\ell_{\max}$ will reduce the statistical error, but the RS contributions will start to deteriorate the parameter accuracy. Fig. 6 depicts the individual conditional statistical and systematical errors as a function of maximum multipole order $\ell_{\max}$. In comparison to the statistical errors on parameters derived with the iSW spectrum, which are monotonically decreasing, the parameter estimation biases due to RS contributions have a more complicated behaviour with multipole order ℓ, but remain always small in comparison to the statistical error by more than one order of magnitude, for both cosmic variance dominated experiments and the combination of *Planck* with *Euclid*. The worst case is the constraint on w in a cosmic variance limited experiment, where the systematic error amounts to 20 per cent of that of the statistical error. There are certain scales at which the systematical errors are very small, namely as they change their signs, in agreement with changing parameter degeneracies on different angular scales.

8 SUMMARY

The topic of this paper is an investigation of the contamination due to non-linearly evolving structures on the linear iSW effect, and the consequent parameter estimation biases.

(i) The angular spectrum of the RS effect was computed in third-order perturbation theory. The spectrum $C_{\tau\tau}(\ell)$ of the RS effect starts dominating that of the linear iSW effect from multipoles of $\ell \simeq 100$ onwards. In particular the cross-spectrum $C_{\tau\gamma}(\ell)$ shows a
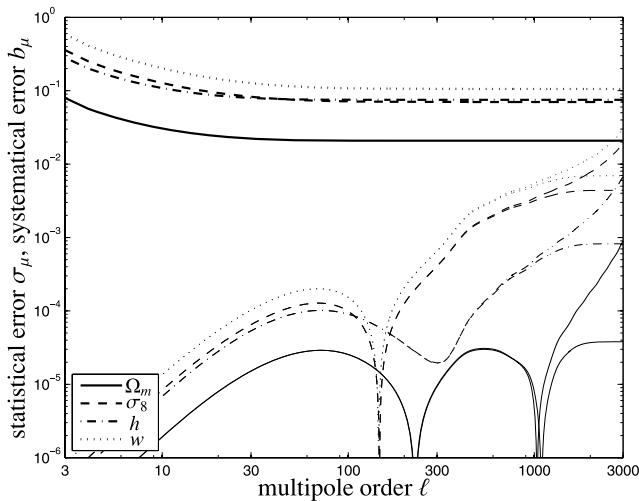
Figure 6. Conditional statistical errors $\sigma_\mu(\ell_{max})$ (thick lines) and systematical errors $b_\mu(\ell_{max})$ (thin lines) for individual cosmological parameters: Ω_m (solid line), σ_8 (dashed line), h (dash–dotted line) and w (dotted line) as a function of maximum multipole order ℓ_{max}. No prior information is used in the computation of the errors. The plot compares a cosmic variance limited measurement (upper lines) with the cross-correlation of *Planck* with *Euclid* (lower lines).

sign change suggesting that the CMB temperature is anticorrelated with the galaxy density on non-linear scales. This scale bears some sensitivity on w and is shifted from $\ell \simeq 70$, where the sign change occurs in the spectrum of the non-linear effect, to $\ell \simeq 500$ for the combination of the linear and non-linear effects. The sensitivity of the RS effect on the dark energy model itself is rather weak.

(ii) By combining the *Planck* and *Euclid* data sets one can measure the non-linear RS effect with a significance of 0.77σ out to multipoles of $\ell = 3000$, where the most important limitations are cosmic variance and *Planck*'s instrumental noise. An ideal experiment only subjected to cosmic variance would be able to detect the effect with 3.22σ, but at higher multipoles, confusion with the kinetic Sunyaev–Zel'dovich effect would occur. Measurements of the angular scale on which the sign change occurs are almost impossible as the signal-to-noise ratio on these scales is $\simeq 10^{-3}$. In summary, the significance of the RS effect is smaller than that of the iSW effect by a factor of ~ 10 for the combination of *Planck* with *Euclid*, which reaches $\sim 7\sigma$.

(iii) If constraints on cosmological parameters are derived from the linear iSW effect and if contributions from the RS effect are neglected, the induced parameter estimation biases are smaller than the statistical errors by one order of magnitude because of the smallness of the RS effect in comparison to cosmic variance induced into the measurement by primary CMB fluctuations and because of the strong prior used. If the iSW effect is used to constrain individual cosmological parameters without using a CMB prior, a similar result still applies. Therefore, the RS effect is negligible as a systematic in comparison to other systematics that have been discussed in the literature and which have a more pronounced effect on cosmological parameters, e.g. redshift errors due to peculiar motion of the tracer galaxies (Rassat 2009), weak lensing on the tracer population and galaxy magnification bias (Loverde, Hui & Gaztañaga 2007), bias evolution of the tracer population (Raccanelli et al. 2008; Schäfer, Douspis & Aghanim 2009) and contributions due to the kinetic Sunyaev–Zel'dovich effect from re-ionization (Giannantonio & Crittenden 2007).

Given the estimates that both the spectrum and the bispectrum of the RS effect are only detectable with significance of $\sim 0.8\sigma$ casts doubt on the detectability of this effect in a statistical way, and emphasizes the importance of alternative approaches such as stacking methods (Granett, Neyrinck & Szapudi 2008).

REFERENCES

Abramowitz M., Stegun I. A., 1972, Handbook of Mathematical Functions. Dover Press, New York
Amara A., Refregier A., 2007, MNRAS, 391, 228
Amara A., Réfrégier A., 2007, MNRAS, 381, 1018
Bardeen J. M., Bond J. R., Kaiser N., Szalay A. S., 1986, ApJ, 304, 15
Bernardeau F., Colombi S., Gaztañaga E., Scoccimarro R., 2002, Phys. Rep., 367, 1
Boughn S., Crittenden R., 2004, Nat, 427, 45
Cabré A., Gaztañaga E., Manera M., Fosalba P., Castander F., 2006, MNRAS, 372, L23
Cabré A., Fosalba P., Gaztañaga E., Manera M., 2007, MNRAS, 381, 1347
Cai Y.-C., Cole S., Jenkins A., Frenk C., 2008, MNRAS, 396, 772
Cai Y., Cole S., Jenkins A., Frenk C. S., 2010, MNRAS, 407, 201
Cooray A., 2002, Phys. Rev. D, 65, 083518
Cooray A., Sheth R., 2002, Phys. Rep., 372, 1
Crittenden R. G., Turok N., 1996, Phys. Rev. Lett., 76, 575
da Silva A. C., Barbosa D., Liddle A. R., Thomas P. A., 2001, MNRAS, 326, 155
Douspis M., Castro P. G., Caprini C., Aghanim N., 2008, A&A, 485, 395
Fosalba P., Gaztañaga E., Castander F. J., 2003, ApJ, 597, L89
Gaztañaga E., Manera M., Multamäki T., 2006, MNRAS, 365, 171
Giannantonio T., Crittenden R., 2007, MNRAS, 381, 819
Giannantonio T. et al., 2006, Phys. Rev. D, 74, 063520
Giannantonio T., Scranton R., Crittenden R. G., Nichol R. C., Boughn S. P., Myers A. D., Richards G. T., 2008, Phys. Rev. D, 77, 123520
Goldberg D. M., Spergel D. N., 1999, Phys. Rev. D, 59, 103002
Granett B. R., Neyrinck M. C., Szapudi I., 2008, ApJ, 683, L99
Ho S., Hirata C., Padmanabhan N., Seljak U., Bahcall N., 2008, Phys. Rev. D, 78, 043519
Hu W., Sugiyama N., 1994, Phys. Rev. D, 50, 627
Knox L., 1995, Phys. Rev. D, 52, 4307
Lewis A., Challinor A., Lasenby A., 2000, ApJ, 538, 473
Limber D. N., 1954, ApJ, 119, 655
Linder E. V., Jenkins A., 2003, MNRAS, 346, 573
Loverde M., Hui L., Gaztañaga E., 2007, Phys. Rev. D, 75, 043519
McEwen J. D., Vielva P., Hobson M. P., Martínez-González E., Lasenby A. N., 2007, MNRAS, 376, 1211
Maturi M., Dolag K., Waelkens A., Springel V., Enßlin T., 2007, A&A, 476, 83
Mollerach S., Gangui A., Lucchin F., Matarrese S., 1995, ApJ, 453, 1
Munshi D., Souradeep T., Starobinsky A. A., 1995, ApJ, 454, 552
Nishizawa A. J., Komatsu E., Yoshida N., Takahashi R., Sugiyama N., 2008, ApJ, 676, L93

Nolta M. R. et al., 2004, ApJ, 608, 10

Padmanabhan N., Hirata C. M., Seljak U., Schlegel D. J., Brinkmann J., Schneider D. P., 2005, Phys. Rev. D, 72, 043525

Pietrobon D., Balbi A., Marinucci D., 2006, Phys. Rev. D, 74, 043524

Raccanelli A., Bonaldi A., Negrello M., Matarrese S., Tormen G., de Zotti G., 2008, MNRAS, 386, 2161

Rassat A., 2009, Phys. Rev. D, submitted (ArXiv:0902.1759)

Rassat A., Land K., Lahav O., Abdalla F. B., 2007, MNRAS, 377, 1085

Rees M. J., Sciama D. W., 1968, Nat, 217, 511

Refregier A. et al. (the DUNE collaboration), 2009, Exp. Astron., 23, 17

Sachs R. K., Wolfe A. M., 1967, ApJ, 147, 73

Sahni V., Coles P., 1995, Phys. Rep., 262, 1

Schäfer B. M., 2008, MNRAS, 388, 1394

Schäfer B. M., Bartelmann M., 2006, MNRAS, 369, 425

Schäfer B. M., Douspis M., Aghanim N., 2009, MNRAS, 397, 925

Seljak U., 1996, ApJ, 460, 549

Smail I., Hogg D. W., Blandford R., Cohen J. G., Edge A. C., Djorgovski S. G., 1995, MNRAS, 277, 1

Smith R. E. et al., 2003, MNRAS, 341, 1311

Smith R. E., Hernandez-Monteagudo C., Seljak U., 2009, Phys. Rev. D, 80, 063528

Spergel D. N., Goldberg D. M., 1999, Phys. Rev. D, 59, 103001

Springel V., White M., Hernquist L., 2001, ApJ, 549, 681

Taburet N., Aghanim N., Douspis M., Langer M., 2009, MNRAS, 392, 1153

Taburet N., Douspis M., Aghanim N., 2010, MNRAS, 404, 1197

Tegmark M., Taylor A. N., Heavens A. F., 1997, ApJ, 480, 22

Tuluie R., Laguna P., Anninos P., 1996, ApJ, 463, 15

Turner M. S., White M., 1997, Phys. Rev. D, 56, 4439

Vielva P., Martínez-González E., Tucci M., 2006, MNRAS, 365, 891

Wang L., Steinhardt P. J., 1998, ApJ, 508, 483

APPENDIX A: NON-LINEAR CORRECTIONS IN PERTURBATION THEORY

Fig. A1 illustrates the validity of the perturbative corrections to $P(k)$ due to non-linear growth, by comparison to the result from N-body data (Smith et al. 2003). Third-order perturbation theory is able to describe the increase in fluctuation amplitude due to non-linear structure formation down to very small scales. One notices a deviation between the N-body result and the perturbation theory amounting to about 20 per cent in the transition region at a few inverse Mpc, corresponding to angular scales of $\ell \simeq 300$, if most of the iSW signal in the cross-correlation function arises at a co-moving redshift of $\chi = 2\,\mathrm{Gpc}\,h^{-1}$, i.e. the maximum of the redshift distribution $p(z)\mathrm{d}z$ used in this work. The higher orders beyond 3 in perturbation theory would correct the difference to the N-body result, and it should be kept in mind that the simulation on which the description by Smith et al. (2003) is based uses slightly different cosmological parameters, most notably higher Ω_m and σ_8.

The remarkable behaviour of the non-linear effect to cause an anticorrelation between the CMB and the tracer density is shown again in Fig. A2, in a logarithmic representation.
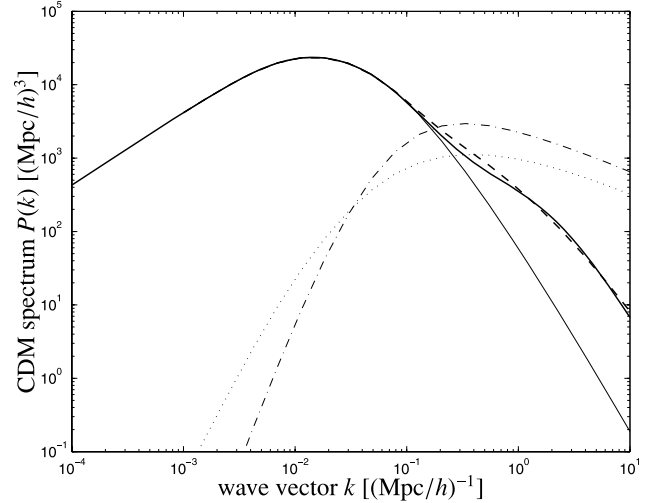

Figure A1. Non-linear corrections to the linear CDM spectrum $P_{\delta\delta}^{(11)}(k)$ (thin solid line) of the density field in perturbation theory, at the current cosmic epoch: $P_{\delta\delta}^{(22)}(k)$ (thin dash–dotted line), the modulus of $P_{\delta\delta}^{(13)}(k)$ (thin dotted line) and their sum $P_{\delta\delta}(k) = P_{\delta\delta}^{(11)}(k) + P_{\delta\delta}^{(22)}(k) + 2P_{\delta\delta}^{(13)}(k)$ (thick dashed line). The fit to the non-linearly evolved spectrum $P_{\delta\delta}(k)$ from N-body data proposed by Smith et al. (2003) is given in comparison (thick solid line).
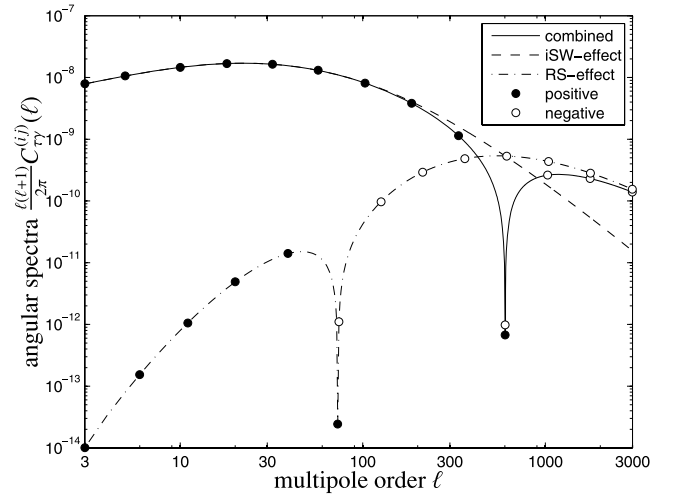

Figure A2. Angular iSW cross-spectrum $C_{\tau\gamma}(\ell)$ of the iSW effect (solid line), split up into the linear effect $C_{\tau\gamma}^{(11)}(\ell)$ (dashed line) and the non-linear RS corrections $C_{\tau\gamma}^{(22)}(\ell) + C_{\tau\gamma}^{(13)}(\ell)$ (dash–dotted line) in logarithmic representation. Open symbols indicate a negative sign and filled symbols a positive sign of the respective branch of the cross-spectrum.

This paper has been typeset from a TEX/LATEX file prepared by the author.